

Supporting Information

Layer-by-Layer Stacked Nanohybrids of N, S-codoped Carbon Film Modified Atomic MoS₂ Nanosheets for Advanced Sodium Dual-ion Batteries

YangJie Liu^{a,b}, Xiang Hu^{a,b}, Guobao Zhong^{a,b}, Junxiang Chen^b, Hongbing Zhan^{a,*}, Zhenhai Wen^{b,*}

^a College of Materials Science and Engineering, Fuzhou University, Fuzhou 350108, China

^b CAS Key Laboratory of Design and Assembly of Functional Nanostructures, and Fujian Provincial Key Laboratory of Nanomaterials, Fujian Institute of Research on the Structure of Matter, Chinese Academy of Sciences, Fuzhou, Fujian 350116, China.

* Corresponding authors: Hongbing Zhan (hbzhan@fzu.edu.cn) and Zhenhai Wen (wen@fjirsm.ac.cn)

Synthesis of a-MoS₂NS@NSC_{film} Nanocomposite:

The K-carrageenan solution (1.3 wt %, 15 mL) was prepared at 70 °C for 1 h to form a homogeneous solution. After that, ammonium thiomolybdate ((NH₄)₂MoS₄) aqueous solution (0.05 mM, 15 mL) was added into the above solution drop by drop to form a reddish brown solution under vigorous stirring. Then, the mixed solution was moved to a 50 mL autoclave and kept at 200 °C for 20 h. After cooling down to room temperature, the obtained precipitate were collect, and dried in an oven at 70 °C. Finally, the as-prepare products were further treated at 800 °C for 2 h under Ar atmosphere with a heating rate of 2 °C min⁻¹. For comparison, the products were prepared with different concentration of K-carrageenan solution (0.66 and 2.0 wt %) and the same amount of ammonium thiomolybdate (200 mg) under the same conditions (named a-MoS₂NS@NSC_{film}-I and a-MoS₂NS@NSC_{film}-III). The pure MoS₂ sample was also fabricated under the same conditions without adding ι-carrageenan.

Characterizations:

The morphologies of the as-obtained samples were performed by FESEM (Hitachi SU-8020), TEM, and HRTEM (Tecnai F20). XRD patterns of the prepared samples were examined on a Miniflex600 powder X-ray diffractometer (XRD) using Cu K α radiation in the 2 θ range from 5° to 70° at a scan rate of 0.05° s⁻¹. Energydispersive X-ray spectroscopy analysis was carried out in the TEM. Nitrogen adsorption–desorption isotherms and Brunauer-Emmett-Teller (BET surface area measurements) were performed with an automated gas sorption analyzer (Hiden IGA100B). The measurements were performed at 77 K, and the pore-size distribution was derived using the density functional theory model. TGA of the sample was recorded with a thermogravimetric analyzer (Netzsch STA449F3) in air with a heating rate of 10 °C min⁻¹ from room temperature to 800 °C. The Raman spectrum was recorded on a Renishaw in Via Raman microscope (532). XPS (ESCALAB 250) was used to determine the components on the surface of the samples.

Electrochemistry Characterization:

The working electrode was fabricated by compressing the slurry mixture of active materials (80 %),

acetylene black (10 %), and sodium carboxymethyl cellulose (10 %) onto a copper foil. The pellets were dried in a vacuum at 100 °C for 24 h, and the 2032 typed coin cells were assembled into a half-battery in an Ar-filled glove box with the concentrations of moisture and oxygen below 1 ppm. Sodium metal was used as the counter/reference electrode, and 1M NaPF₆ in ethylene carbonate (EC) and propylene carbonate (PC) (1:1, v/v) with 5 % fluoroethylene carbonate (FEC) as the electrolyte. What man glass microfiber was used as the separator. The loading mass of the active material was about 1.5 mg cm⁻². The galvanostatic charge–discharge tests were measured with a LAND test system at varied current densities (Wuhan Kingnuo Electronic Co., China) at room temperature, and the voltage range was from 0.01 to 3.0 V. The CV profile was recorded with a CHI660E electrochemical workstation at a scan rate of 0.1 mV s⁻¹. An AC voltage amplitude of 5.0 mV was employed to measure EIS within the frequency range from 10 mHz to 100 kHz. For the long-term cycling performance at high current densities, the half-cell was first activated at 0.1 A g⁻¹ for 3 cycles and then was worked at high current densities for long cycle test. For the Sodium based dual-ion batteries test, as-prepared a-MoS₂NS@NSC_{film}-II samples, EG, and glass fiber were used as anode, cathode and separator, respectively. The electrolyte with composition of 1M NaPF₆ in ethylene carbonate/ethyl methyl carbonate/dimethyl carbonate (EC/EMC/DMC, 1:1:1, v/v/v) was used in dual-ion cells. The mass loading of the anode (a-MoS₂NS@NSC_{film}-II) and cathode (EG) are ≈ 1.5 mg cm⁻² and ≈ 2 mg cm⁻² respectively. The measurement of the cells was similar with half-cells. To characterize the SEM tests, the cells were disassembled inside an argon-filled glove box and the electrodes were washed in propylene carbonate solvent for several times to remove the electrolyte.

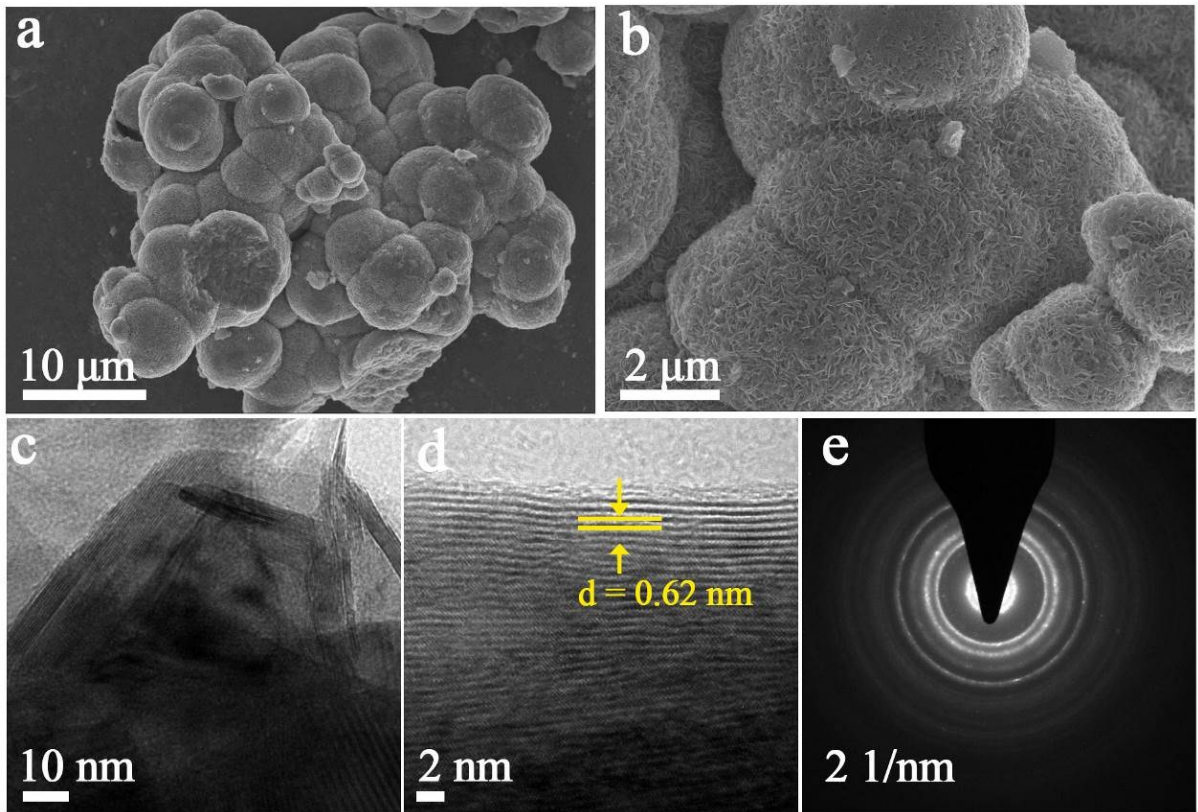


Figure S1. (a, b) FESEM, (c, d) TEM, and (e) SAED images of pure MoS₂ sample.

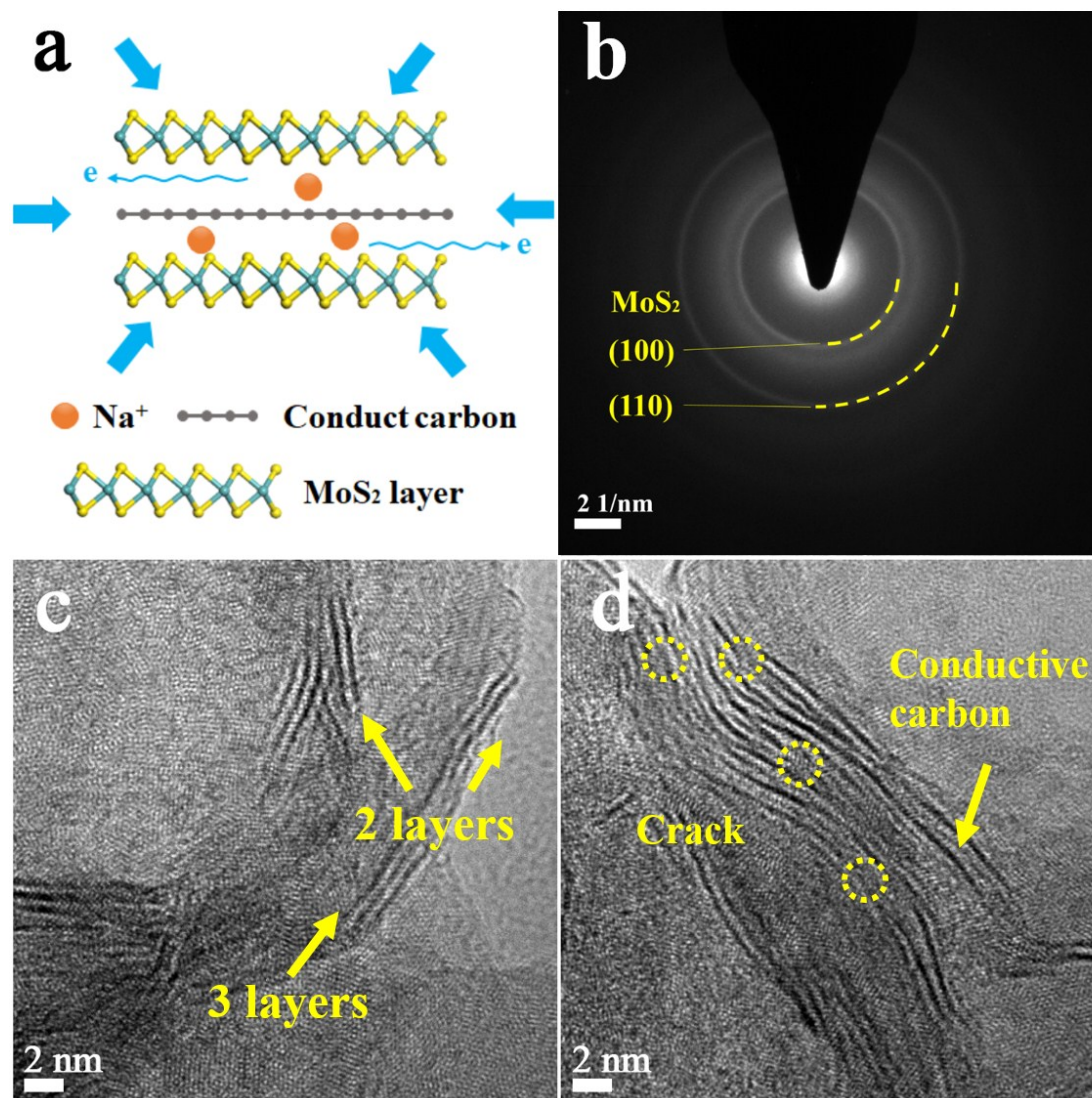


Figure S2. (a) Structural models and (b, c, d) HRTEM images of the a-MoS₂NS@NSC_{film}-II nanocomposites.

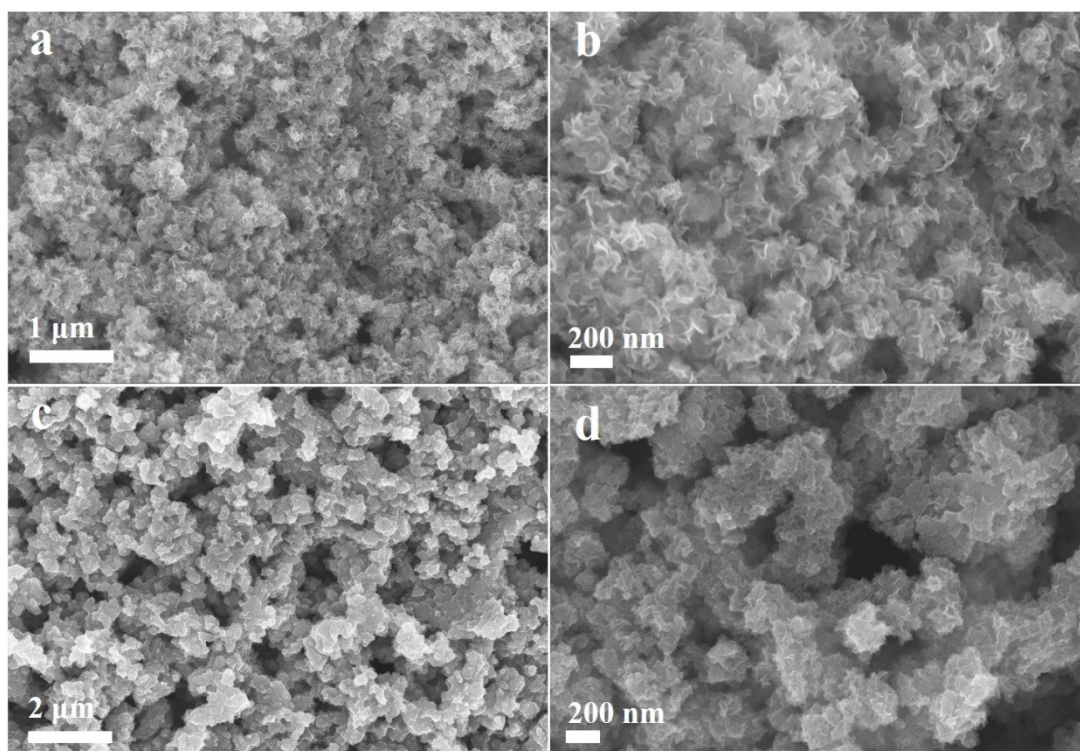


Figure S3. SEM images of (a, b) a-MoS₂NS@NSC_{film-I} and (c, d) a-MoS₂NS@NSC_{film-III}.

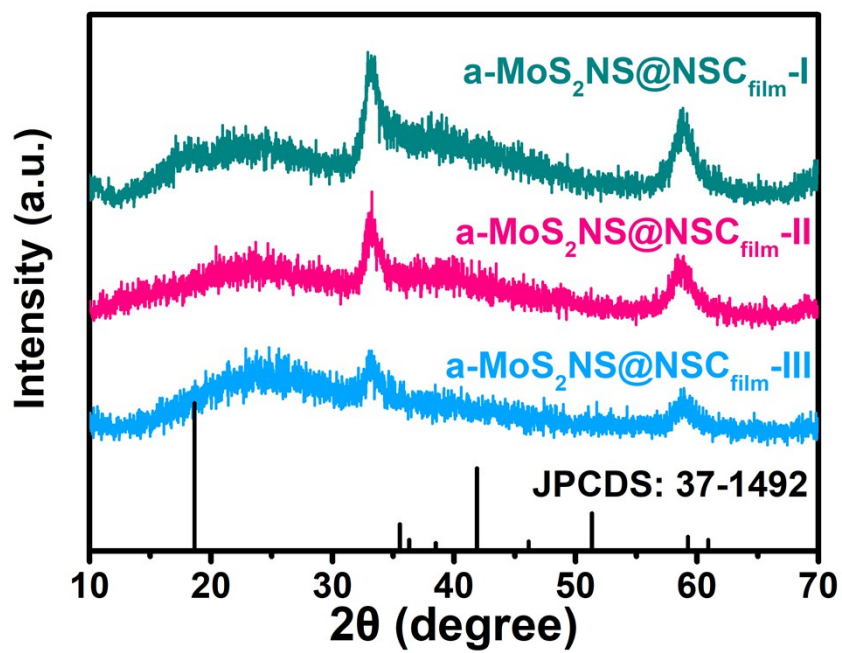


Figure S4. XRD pattern of the $a\text{-MoS}_2\text{NS@NSC}_{\text{film}}$ samples.

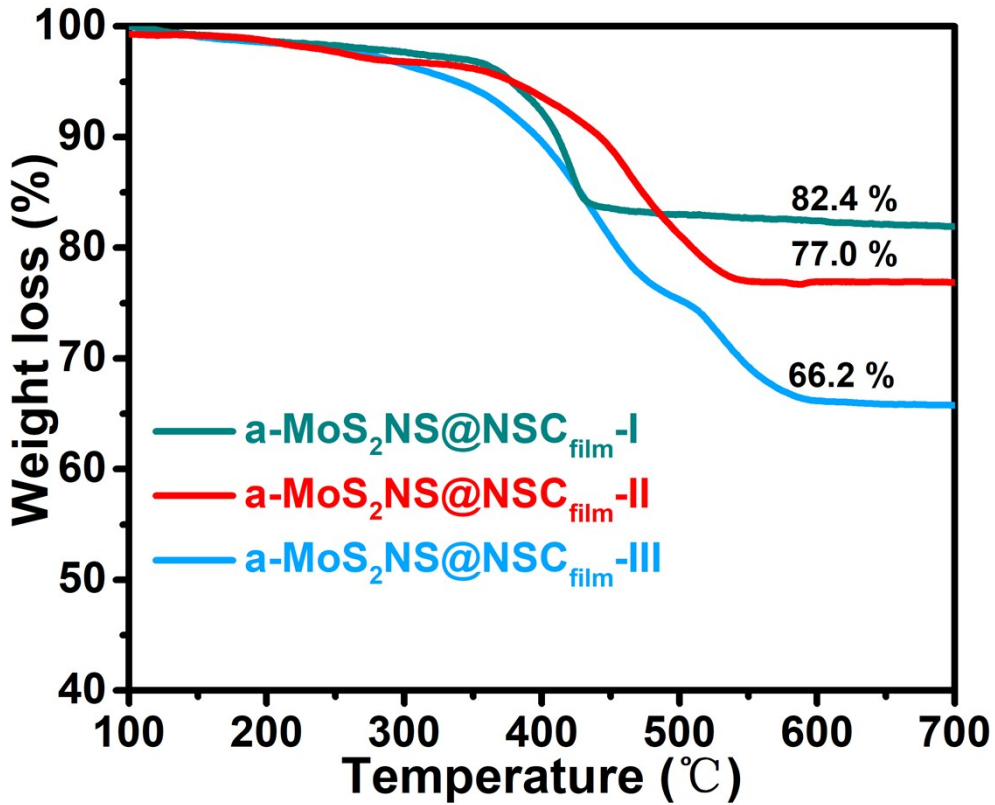


Figure S5. TGA curves of pure MoS₂ and a-MoS₂NS@NSC_{film} samples under air atmosphere in the temperature range of 30 to 700 °C with a heating rate of 10 °C min⁻¹.

An initial mass loss occurs below 300 °C is attributed to the evaporation and desorption of surface adsorbed water molecules, while the second weight loss between 300–600 °C is attributed to the oxidation of MoS₂ to MoO₃ ($2\text{MoS}_2 + 7\text{O}_2 = 2\text{MoO}_3 + 4\text{SO}_2$) and the decomposition of carbon. As viewed in Figure S5, the residual weight percent of a-MoS₂NS@NSC_{film}-I, a-MoS₂NS@NSC_{film}-II and a-MoS₂NS@NSC_{film}-III at 600 °C is 82.4%, 77.0% and 66.2%, respectively. The content of MoS₂ (ω_{MoS_2}) in the a-MoS₂NS@NSC_{film} samples is calculated from the following equation:

$$\omega_{\text{MoS}_2} = \frac{M_{\text{MoS}_2}}{M_{\text{MoO}_3}} * \omega_{\text{MoO}_3}$$

The MoS₂ content in a-MoS₂NS@NSC_{film}-I, a-MoS₂NS@NSC_{film}-II and a-MoS₂NS@NSC_{film}-III is 91.5 %, 85.5 % and 73.5 %, respectively. According to those results, the corresponding carbon content of the three samples are calculated to 8.5 %, 14.5 %, and 26.5 %, respectively.

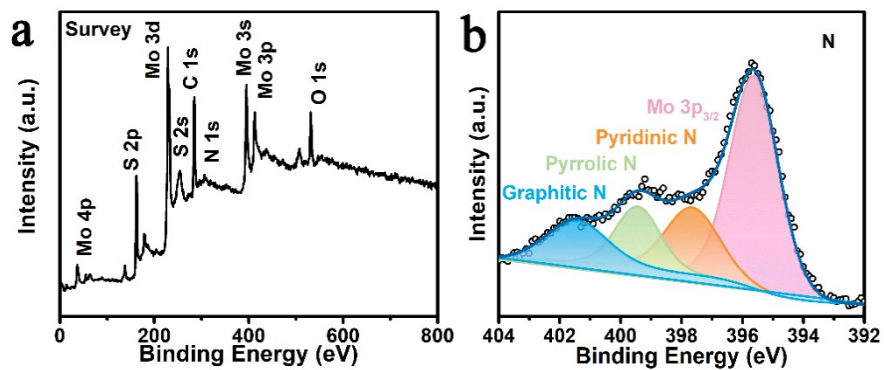


Figure S6. (a) XPS survey scan and (b) high-resolution XPS spectra for N 1s of a-MoS₂NS@NSC_{film}-II nanocomposites.

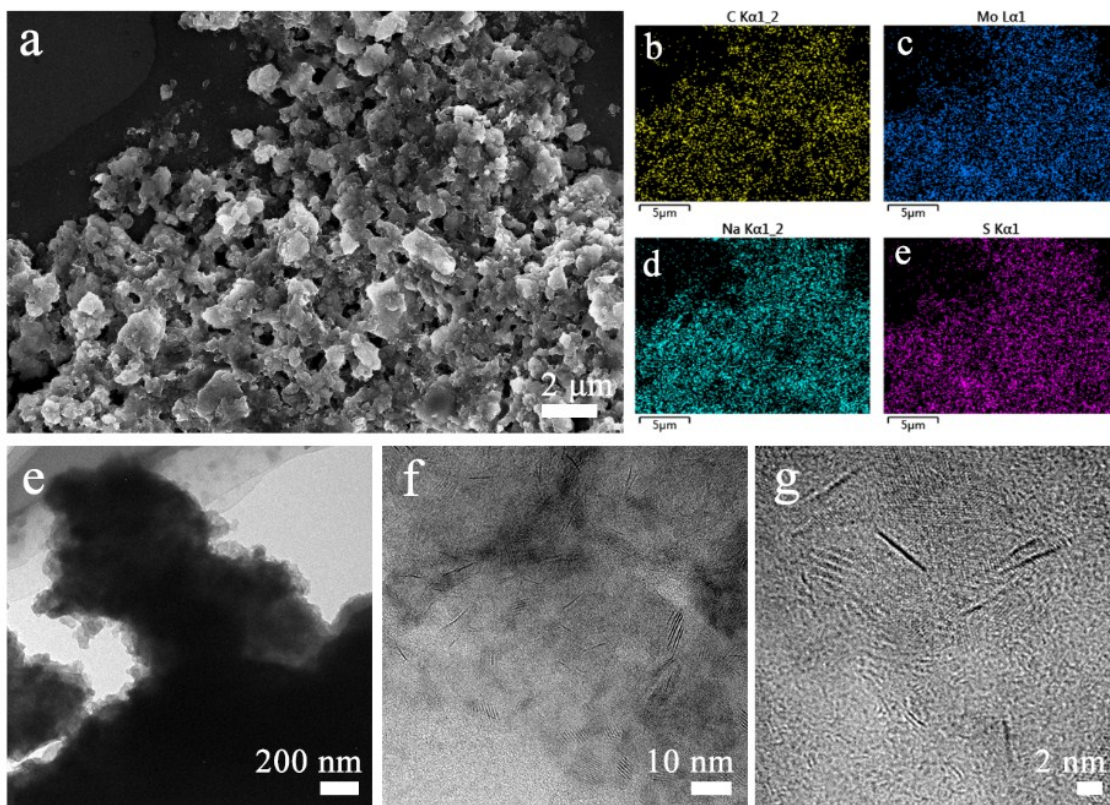


Figure. S7 (a) SEM images, (b-e) SEM EDX mapping images (C, Mo, Na, S) and (c-f) TEM images of the electrode of the a-MoS₂NS@NSC_{film}-II nanocomposite as anode for SIBs after cycling tests.

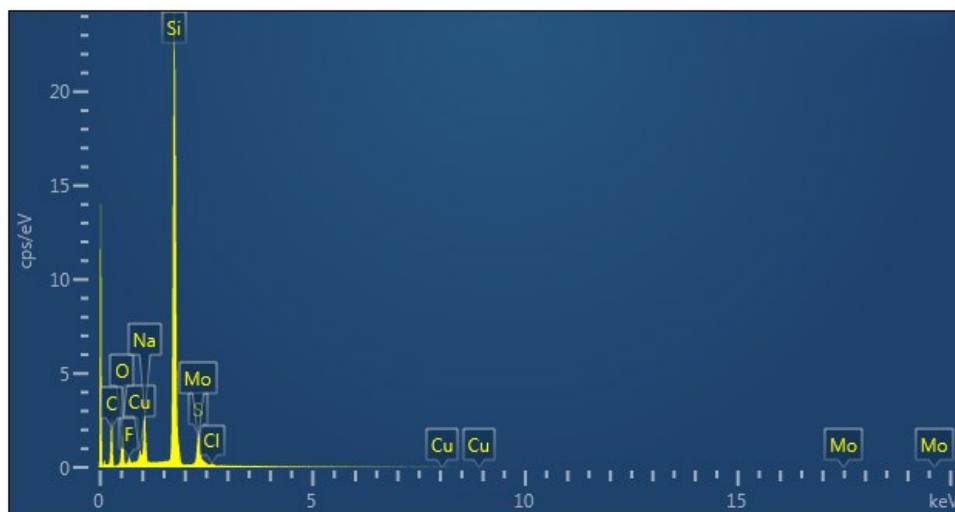


Figure S8. EDS spectra of the a-MoS₂NS@NSC_{film}-II electrode for SIBs after cycling tests.

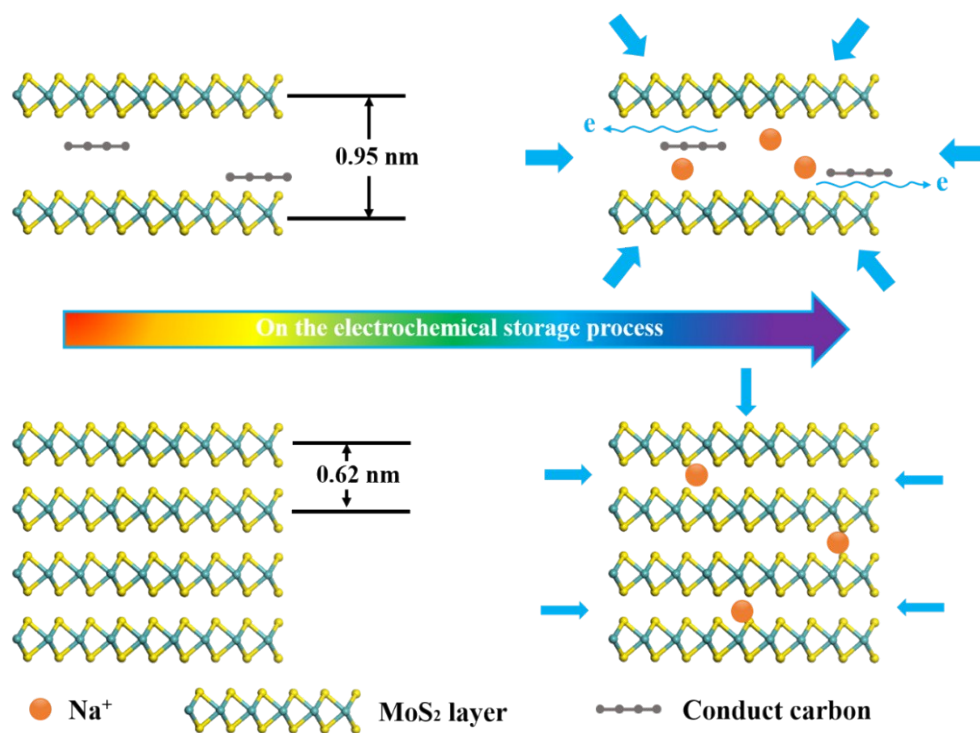


Figure S9. Schematic for the electrochemical reactions involved in the a-MoS₂NS@NSC_{film}-II and pure MoS₂ at different discharge/charge rates.

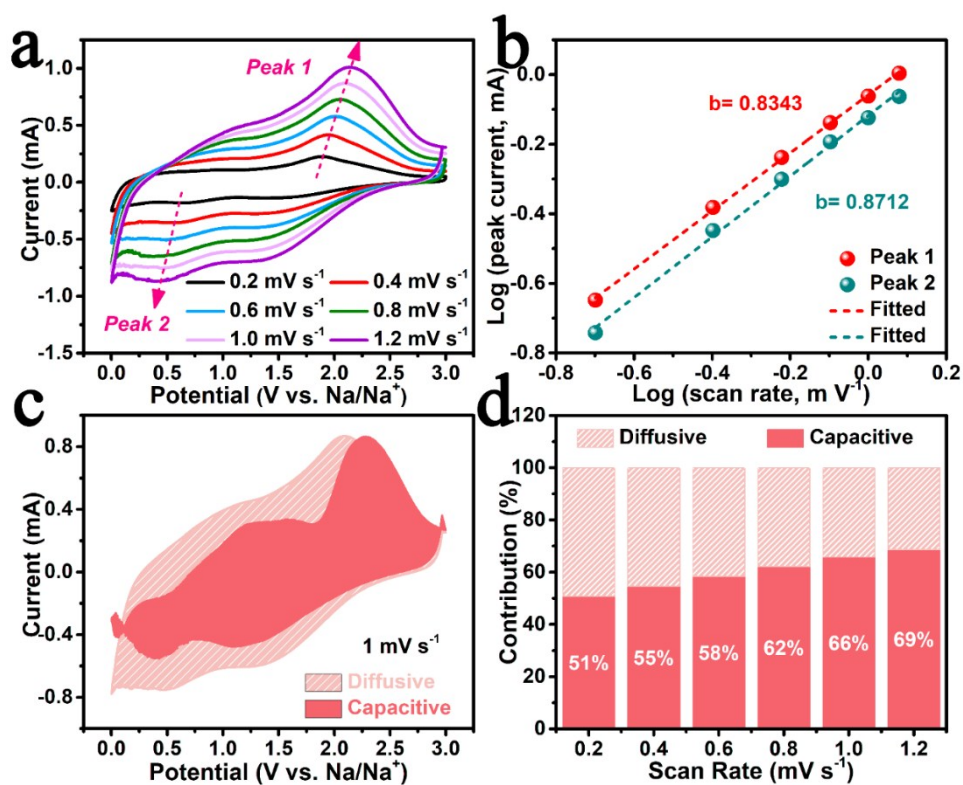


Figure S10. (a) CV curves at different scan rates from 0.2 to 1.2 mV s⁻¹. (b) Log (peak current, A) versus log (sweep rate, mVs⁻¹) plots and the corresponding fitting line. (c) Capacitive and diffusion-controlled contribution to sodium storage of pure MoS₂ at 1 mV s⁻¹. (d) Normalized contribution ratio of capacitive and diffusion-controlled capacities at different scan rates.

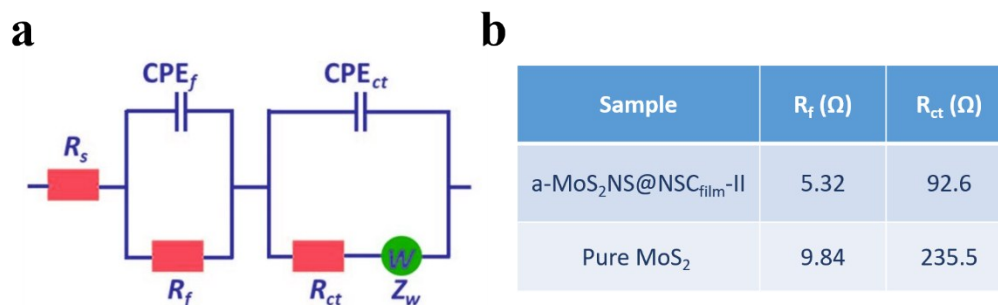


Figure S11. (a) Equivalent circuit model of EIS spectra. (b) The EIS fitting parameters of the a-MoS₂NS@NSC_{film}-II and pure MoS₂ samples.

The equivalent circuit of EIS spectra was provided to fit the Nyquist plots. In brief, R_s , R_f , R_{ct} , and Z_w denote the total ohmic resistance of the electrolyte and electrode, SEI resistance, charge-transfer resistance and Warburg impedance, respectively. CPE_f and CPE_{ct} are the surface capacitance and double layer capacitance, respectively

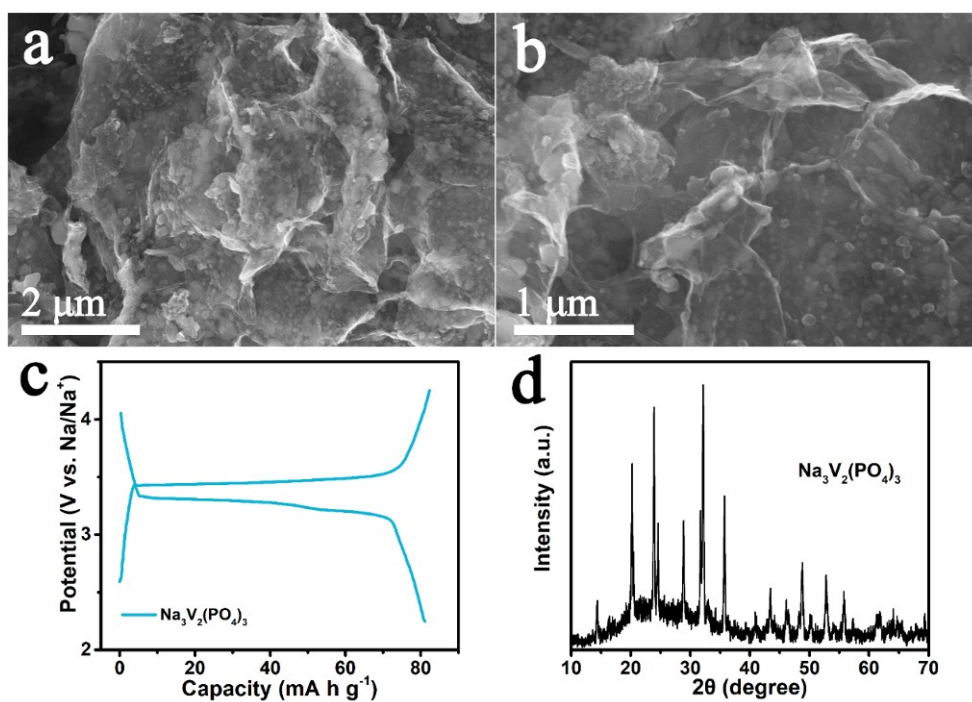


Figure S12. (a, b) SEM images and. (c) First three charge-discharge profiles at 0.1 A g^{-1} of $\text{Na}_3\text{V}_2(\text{PO}_4)_3$ cathode and (d) XRD pattern of the $\text{Na}_3\text{V}_2(\text{PO}_4)_3$.

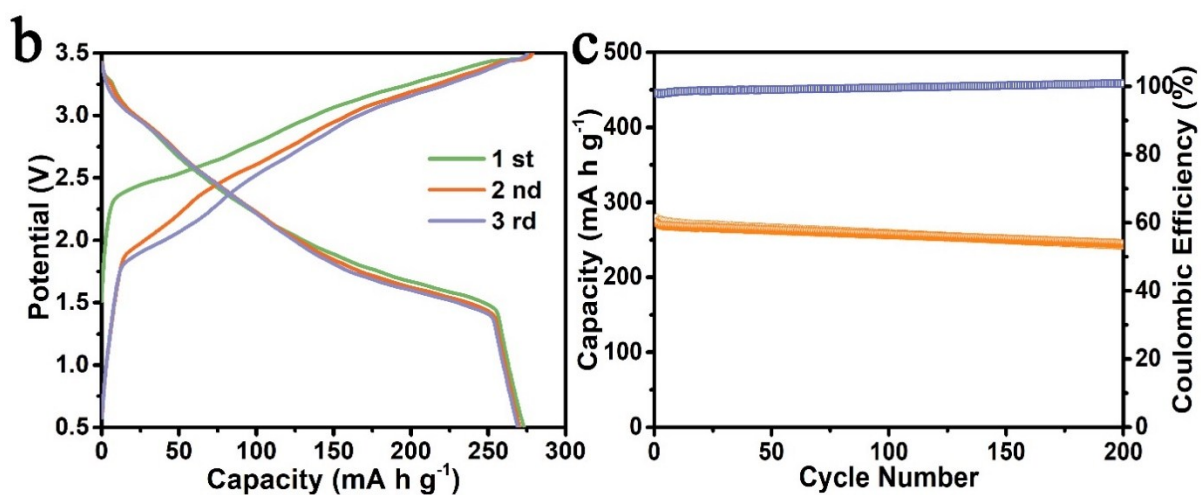
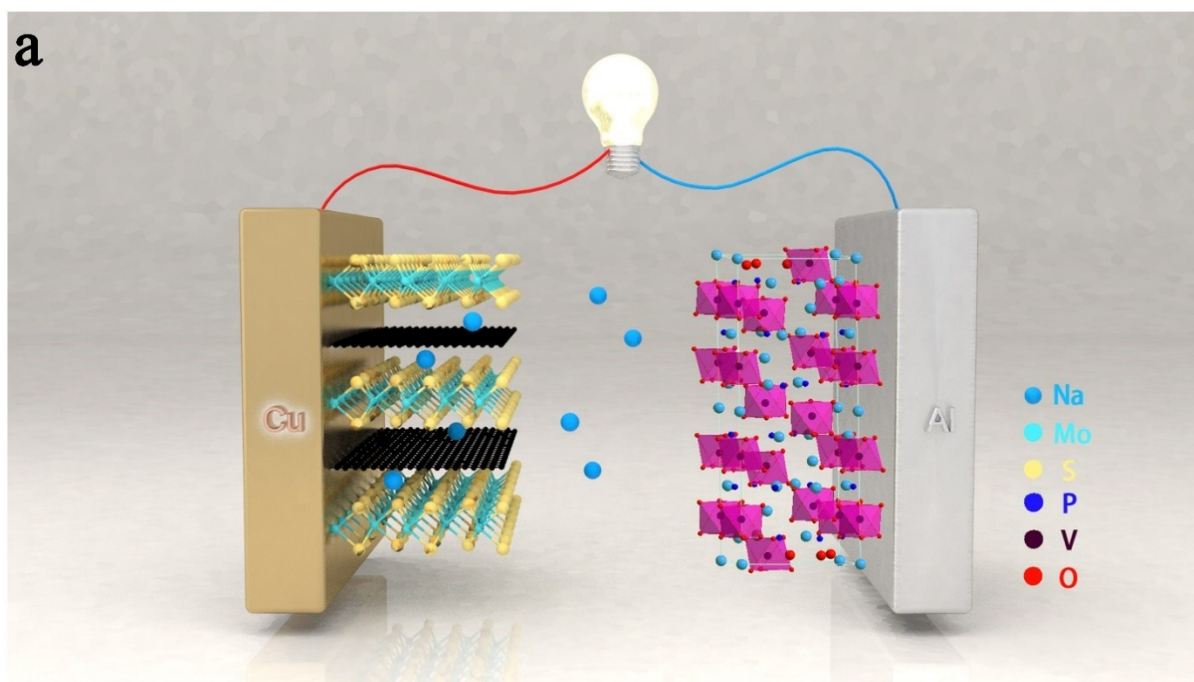


Figure S13. a) Schematic illustration of the full sodium-ion cell with a-MoS₂NS@NSC_{film}-II/Na₃V₂(PO₄)₃ couple. b) Charge and discharge curves and c) cycling performance of the full cell at 0.2 A g⁻¹ (based on the mass of anode).

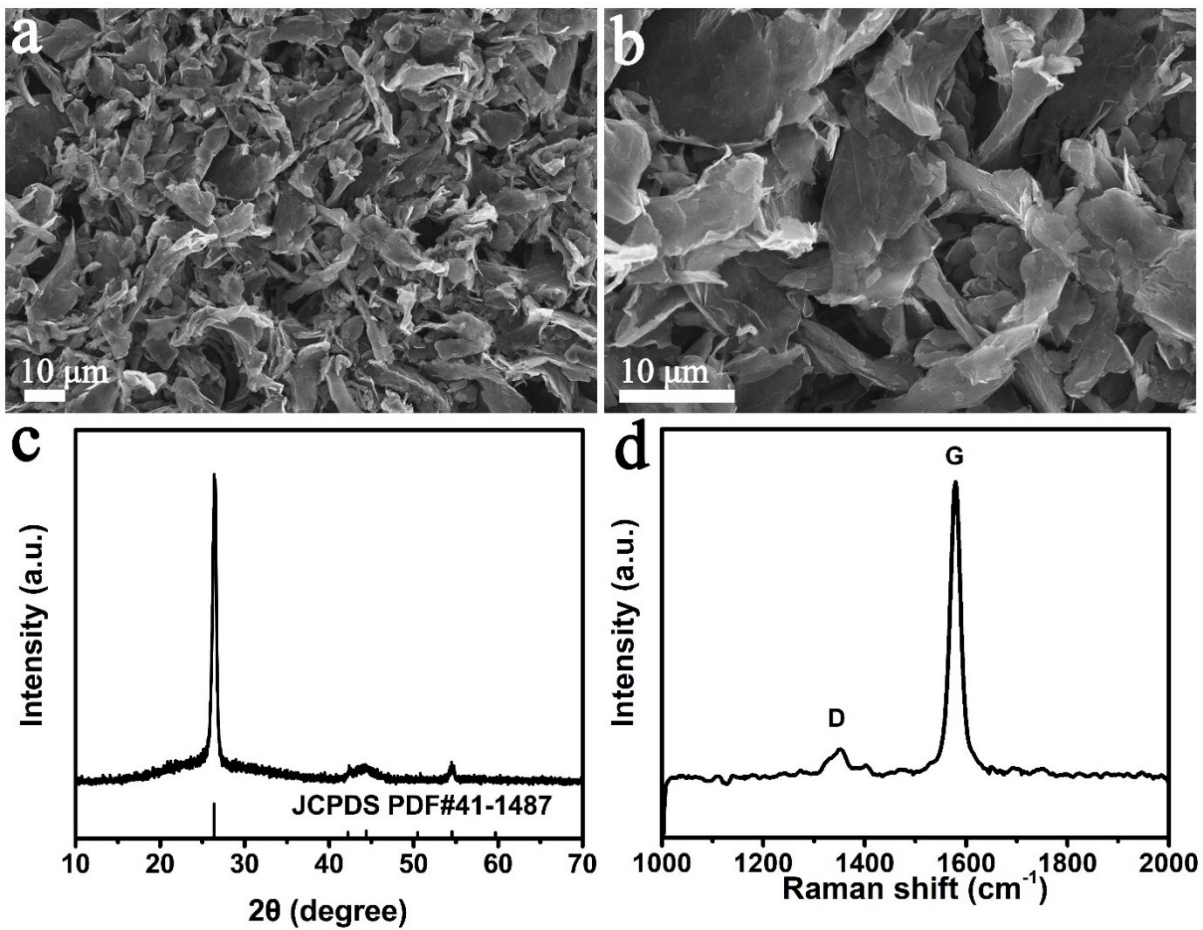


Figure S14. (a-b) FE-SEM images of EG shows a structure of sheet-like morphology. (c) XRD peaks are fully indexed to the graphite-2H peaks (JCPDS card no. 00-041-1487). (d) Raman spectrum suggest that the EG has a stronger G band with a weak D-band.

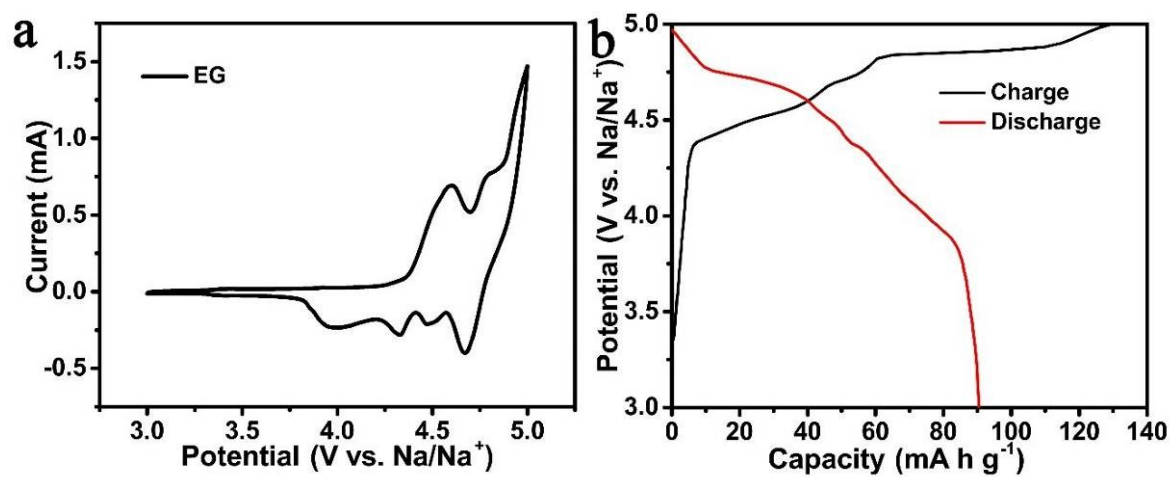


Figure S15. (a) Cyclic voltammetry curves and (b) galvanostatic charge-discharge curves of the dual-ion battery based on EG cathode and Na foil anode at a current density of 0.1 A g⁻¹.

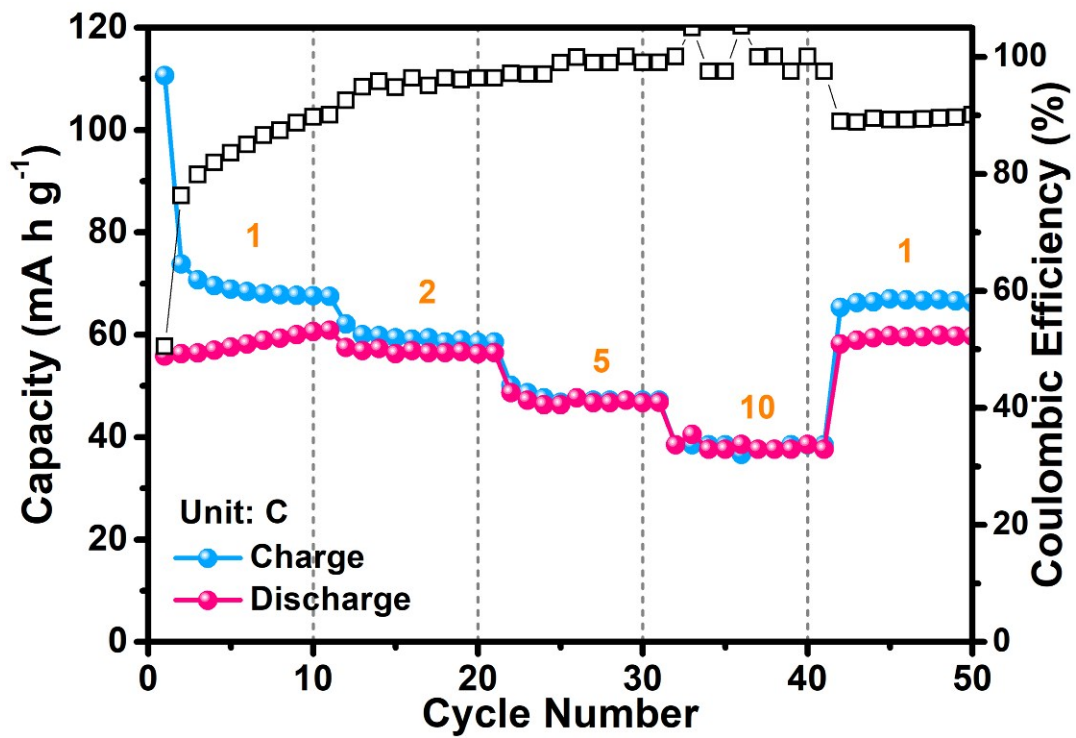


Figure S16. Rate performance of a-MoS₂NS@NSC_{film-II}//EG SDIBs at various current density at 1, 2, 5 and 10 C.

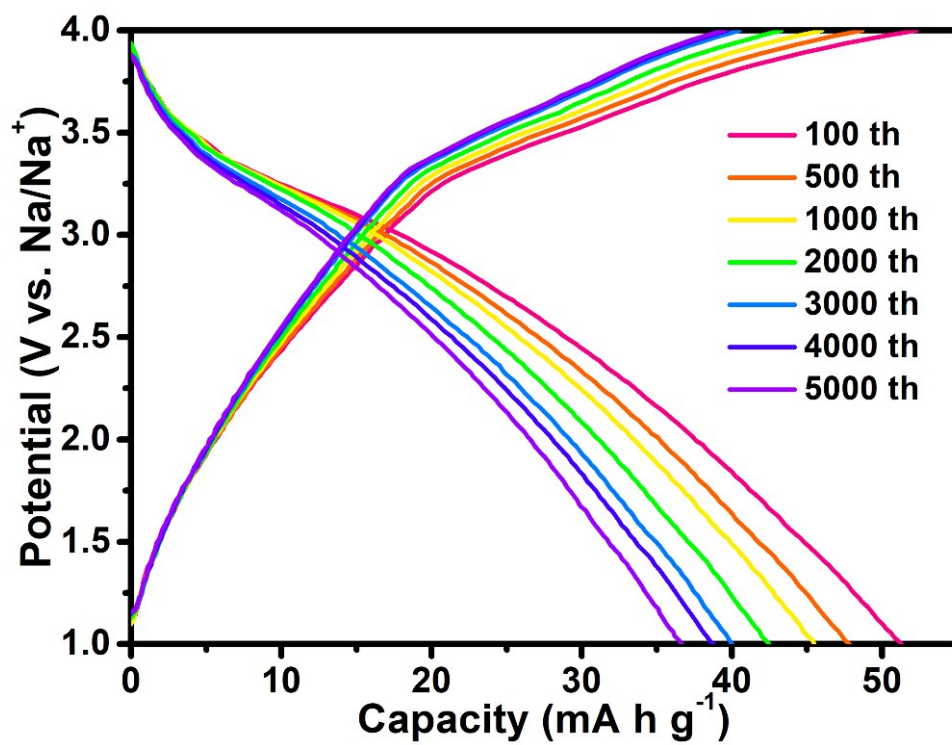


Figure S17. Galvanostatic charge/discharge profiles of the SDIBs at the different cycles at 10 C.

Table S1. Gravimetric performance comparison of this work versus the reported MoS₂-based anode materials in SIBs.

Sample	Current density (A g ⁻¹)	Initial discharge/charge capacity (mA h g ⁻¹)	Reversible capacity (mA h g ⁻¹)/Cycles/Current density (A g ⁻¹)	References
a-MoS ₂ NS@NSC _{film} -II	0.1	857/641	492/100/0.1	This work
			298/500/1	
HMF-MoS ₂	0.1	694/418	384/100/0.1	1
US-MoS ₂ @NG	0.1	416/280	198/1000/1	2
MoS ₂ /Graphene	0.1	890/484	432/100/0.1	3
MoS ₂ @C-CMC paper electrode	0.08	450/360	286/100/0.1	4
MoS ₂ @NOC	0.1	610/490	419/100/0.1	5
MoS ₂ @Carbonfiber	0.05	490/319	241/700/1	6
MoS ₂ /C	0.1	690/360	343/100/0.1	7
MoS ₂ /SnO ₂ /C	0.1	530/340	230/450/1	8
MoS ₂ @CNFs	0.1	1238/617	500/80/0.1	9
MoS ₂ Microflowers	0.1	720/600	500/100/0.1	10

Table S2. Gravimetric performance comparison of this work versus the reported anode of SDIBs.

Sample	Reversible capacity (mA h g ⁻¹)/Cycles/Current density (A g ⁻¹)	References
a-MoS ₂ NS@NSC _{film} -II//EG	62.5/300/0.1	This work
	39.3/5000/1	
Penne-Like MoS ₂ /Carbon//EG	65/100/0.1	11
	55/200/0.2	
MoS ₂ @N-Hollow spheres//EG	40/500/1	12
MoS ₂ flowers//EG	39.7/300/0.4	13
Soft carbon//EG	56.6/350/0.1	14
Exfoliated graphene//exfoliated graphene	61/200/0.05	15
Sn foil//graphite	70/400/0.2	16

Table S3. Comparison of the initial coulombic efficiency of the other reported DIBs systems with our work under low current rate.

Materials	Current density (A g ⁻¹)	Initial coulombic efficiency (%)	Coulombic efficiency after cycles	Reference
a-MoS ₂ NS@NSC _{film} //EG (Sodium-DIBs)	0.1	58.2	95.6% (300 th)	This work
(MoS ₂ /CF)@MoS ₂ @C//EG (Sodium-DIBs)	0.2	66.1	≈ 93% (50 th)	<i>Energy Storage Mater.</i> 2018 , 15, 22–30
MoS ₂ /C nanotubes//EG (Sodium-DIBs)	0.2	48.0	≈ 90% (200 th)	<i>Small</i> , 2018 , 14, 1703951
pAl/C//natural graphite (Sodium-DIBs)	0.2	53.2	93.1% (1000 th)	<i>Adv. Mater.</i> 2016 , 28, 9979-9985
Sn foil//EG (Potassium-DIBs)	0.05	48.5	85% (300 th)	<i>Adv. Mater.</i> 2017 , 29, 1700519
mesocarbon microbead//EG (Potassium-DIBs)	0.1	42.3	≈ 95% (100 th)	<i>Adv. Energy Mater.</i> 2017 , 7, 1700920
nAl@C//EG (Lithium-DIBs)	0.2	58.0	93% (1000 th)	<i>Adv. Energy Mater.</i> 2018 , 8, 1701967
Al//mesocarbon microbead (Lithium-DIBs)	0.5	33.0	≈ 90% (300 th)	<i>Adv. Mater. Interfaces</i> 2016 , 3, 1600605

References

1. Z. Chen, D. Yin and M. Zhang, *Small*, 2018, **14**, 1703818.
2. H. Yang, M. Wang, X. W. Liu, Y. Jiang and Y. Yu, *Nano Res.*, 2018, **11**, 3844-3853.
3. Z. H. Zhao, X. D. Hu, H. Wang, M. Y. Ye, Z. Y. Sang, H.-M. Ji, X. L. Li and Y. Dai, *Nano Energy*, 2018, **48**, 526-535.
4. C. Zhao, C. Yu, M. Zhang, Q. Sun, S. Li, M. Norouzi Banis, X. Han, Q. Dong, J. Yang, G. Wang, X. Sun and J. Qiu, *Nano Energy*, 2017, **41**, 66-74.
5. M. Han, Z. Lin and J. Yu, *J. Mater. Chem. A*, 2019, **7**, 4804-4812.
6. X. Q. Xie, T. Makaryan, M. Q. Zhao, K. L. Van Aken, Y. Gogotsi and G. X. Wang, *Adv. Energy Mater.*, 2016, **6**, 1502161.
7. D. Sun, D. Ye, P. Liu, Y. Tang, J. Guo, L. Wang and H. Wang, *Adv. Energy Mater.*, 2018, **8**, 1702383.
8. X. Xu, R. Zhao, W. Ai, B. Chen, H. Du, L. Wu, H. Zhang, W. Huang and T. Yu, *Adv. Mater.*, 2018, **30**, 1800658.
9. Y. Li, R. Zhang, W. Zhou, X. Wu, H. Zhang and J. Zhang, *ACS Nano*, 2019, **13**, 5533-5540.
10. S. Anwer, Y. Huang, B. Li, B. Govindan, K. Liao, J. C. W, F. Wu, R. Chen and L. Zheng, *ACS Appl. Mater. Interfaces*, 2019, **11**, 22323-22331.
11. H. Zhu, F. Zhang, J. Li and Y. Tang, *Small*, 2018, **14**, 1703951.
12. Z. Y. Li, L. W. Yang, G. B. Xu, X. Liu, X. L. Wei, J. X. Cao and P. K. Chu, *ChemElectroChem*, 2019, **6**, 661-667.
13. J. Fan, Q. Xiao, Y. Fang, L. Li, W. Feng and W. Yuan, *ChemElectroChem*, 2018, **6**, 676-683.
14. X. Yao, Y. Ke, W. Ren, X. Wang, F. Xiong, W. Yang, M. Qin, Q. Li and L. Mai, *Adv. Energy Mater.*, 2018, **9**, 1803260.
15. F. Wang, Z. Liu, P. Zhang, H. Li, W. Sheng, T. Zhang, R. Jordan, Y. Wu, X. Zhuang and X. Feng, *Small*, 2017, **13**, 1702449.
16. M. H. Sheng, F. Zhang, B. F. Ji, X. F. Tong and Y. B. Tang, *Adv. Energy Mater.*, 2017, **7**, 1601963.